Right ventromedial and dorsolateral prefrontal cortices mediate adaptive decisions under ambiguity by integrating choice utility and outcome evaluation.

Anastasia Christakou, Mick Brammer, Vincent Giampietro, Katya Rubia

Supplemental Material

METHODS

A. Individual Level Analysis

fMRI data were realigned to minimise motion-related artefacts (Bullmore et al., 1999b), and smoothed using a Gaussian filter (full-width half maximum, 8.82 mm). Time-series analysis of individual subject activation was performed using XBAM v4, with a wavelet-based re-sampling method previously described (Bullmore et al., 2001). Briefly, we first convolved each experimental condition (choice phase (choice contrasts): disadvantageous / advantageous choices; outcome phase (outcome contrasts): wins / losses), with two Poisson model functions (delays of 4 and 8 s). We calculated the weighted sum of these two convolutions that gave the best fit (least-squares) to the time series at each voxel. A goodness-of-fit statistic (the SSQ-ratio) was then computed at each voxel consisting of the ratio of the sum of squares of deviations from the mean intensity value due to the model (fitted time series), divided by the sum of squares due to the residuals (original time series minus model time series). The appropriate null distribution for assessing significance of any given SSQ-ratio was established using the wavelet-based data re-sampling method (Bullmore et al., 2001), and applying the model-fitting process to the re-sampled data. This process was repeated 20 times at each voxel and the data combined over all voxels, resulting in 20 null parametric maps of SSQ-ratio for each subject, which were combined to give the overall null distribution of SSQ-ratio. The same permutation strategy was applied at each voxel to preserve spatial correlation structure in the data. Instead of relying on asymptotic distributions such as t or F that assume data normality, we use data-driven, permutation-based methods with minimal distributional assumptions that have been shown to be more suitable for fMRI data analysis in samples sizes similar to the ours (Zhang et al., 2009). Activation in the choice phase associated with disadvantageous trials was contrasted with activation associated with advantageous trials. Activation in the outcome phase associated with win trials was contrasted with activation associated with loss trials. Individual SSQ-ratio maps were transformed into standard space, first by rigid body transformation of the fMRI data into a high-resolution inversion recovery image of the same subject, and then by affine transformation onto a Talairach template (Talairach and Tournoux, 1988).

B. Group Level Analysis

A generic activation group map was produced for each experimental condition (choice phase: disadvantageous/advantageous choices; outcome phase: wins/losses), by calculating the median observed SSQ-ratio over all subjects at each voxel in standard space and testing them against the null distribution of median SSQ-ratios computed from the identically transformed wavelet re-sampled (permuted) data (Brammer et al., 1997). The voxel-level threshold was first set to 0.05 to give maximum sensitivity and to avoid type II errors. Next, a cluster-mass threshold was computed from the distribution of cluster masses in the wavelet-permuted data such that the final expected number of type I error clusters under the null hypothesis was <1 per whole brain. Cluster mass rather than a cluster extent threshold was used, to minimise discrimination against possible small, strongly responding foci of activation (Bullmore et al., 1999a).

C. Whole-brain Correlation of Brain Activation with Performance

The Pearson product-moment correlation coefficient was first computed at each voxel in standard space between net score and signal change over all subjects. The correlation coefficients were recalculated after randomly permuting the behavioural (but not the fMRI) data. Repeating the second step many times (1,000 times per voxel, then combining over all voxels) gives the distribution of correlation coefficients under the null hypothesis that there is no association between specific net score values and specific BOLD effects. This null distribution can then be used to assess the probability of any particular correlation coefficient under the null hypothesis. The critical value of the correlation coefficient at any desired type I error level in the original (non-permuted) data can be determined by reference to this distribution. Statistical analysis was extended to cluster level as described by Bullmore and colleagues (Bullmore et al., 1999a). The cluster probability under the null hypothesis was chosen to set the level of expected type I error clusters at an acceptable level (i.e. < 1 per whole brain).

RESULTS

Figure 1. Main Contrasts

A. Choice Contrast

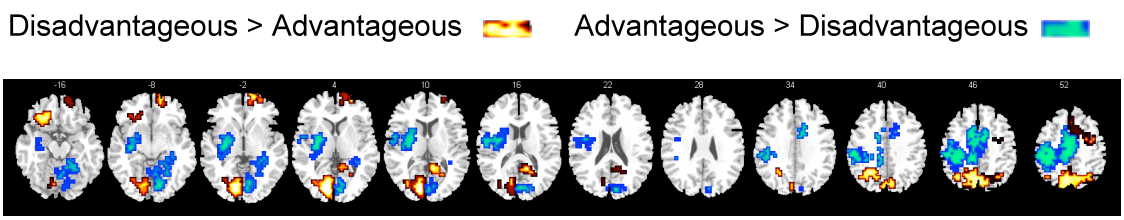

The choice contrast of disadvantageous minus advantageous trials showed activation in left ventrolateral prefrontal cortex (BA47), right ventromedial (BA10) and left visual cortex, SMA, premotor, parietal and posterior cingulate cortices, left cerebellum and occipital cortex. This result replicates previous findings with a similar fMRI adaptation of the IGT [(Lawrence et al., 2008), Figure 2].

A widespread network of areas was activated during advantageous compared to disadvantageous choices, including motor cortex, postcentral gyrus, cingulate and bilateral temporal cortex, striatum, pallidum, thalamus, amygdala and hippocampus. We tested the correlation of the SSQ ratio of the difference in activation of these clusters with performance, and found that a single cluster in the dorsal cingulate gyrus (BA24) survived correction in its correlation with net score (x=-11, y=4, z=42; size=54 voxels; r=0.72, p<0.001).

B. Outcome Contrast

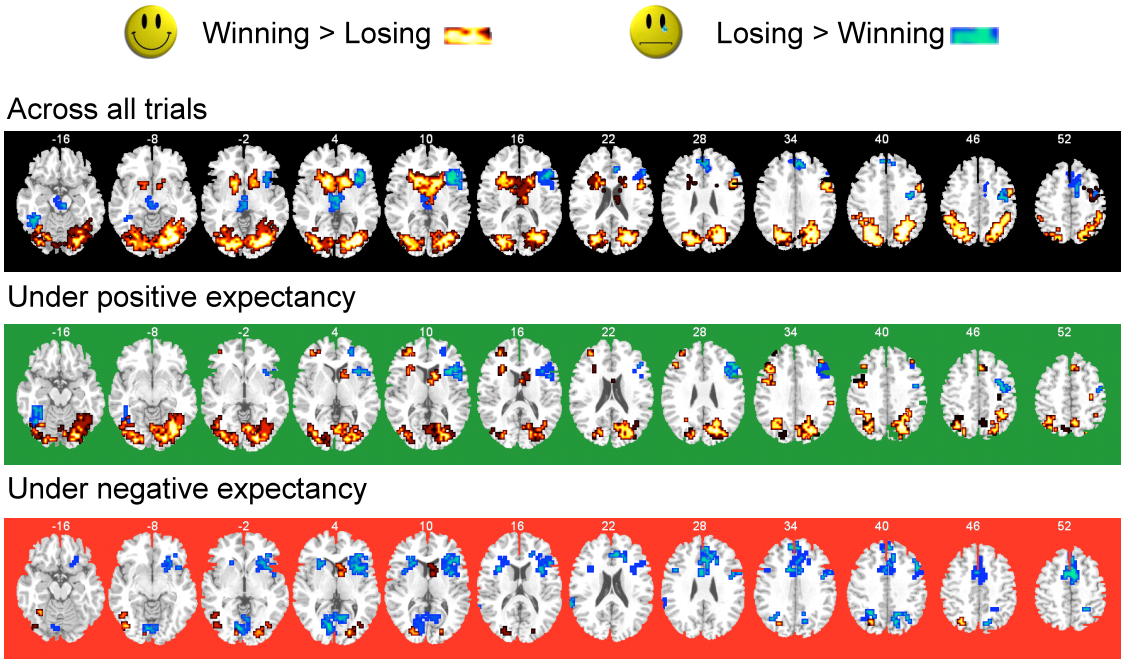

Areas responding more to wins than losses (red-yellow palette), and to losses than wins (blue-green palette): (Top Panel) Across all trials; (Middle Panel) Areas sensitive to the level of expected value (EV) of the trial, when EV was

positive (positive expectancy); (Bottom Panel) Areas sensitive to the EV of the trial when EV was negative (negative expectancy). 3D clusters of activation for the two contrasts are presented superimposed on horizontal slices, marked with the Z coordinate as distance in millimetres from the anterior-posterior commissure.

Across the whole session (top panel), win compared to loss trials showed increased activation in caudate, right dorsolateral prefrontal, parietal and visual cortex (red palette). Conversely, loss trials showed increased activation in right insula, ACC, dmPFC and right dlPFC, pre-SMA, fusiform gyrus, thalamus and midbrain (blue palette).

The bottom two panels show group maps of the contrast between wins and losses in voxels where activity was modulated by EV. Clusters that were sensitive to positive expectancy (middle panel) and responded more to wins than losses (red palette) were located in left lateral prefrontal and dorsomedial fontal cortices, caudate, and posterior parietal and visual areas. Loss compared to win trials (blue palette) activated right anterior insula, dlPFC, precentral, and fusifom gyrus. By contrast, clusters that were sensitive to negative expectancy (bottom panel), showed increased activation during wins compared to losses (red palette) in significantly more confined visual and parietal areas, while increased activation during losses compared to wins (blue palette) was enhanced: the right insula activation observed before was more extensive and extended into the right vlPFC, while additional clusters were observed in the left insula/claustrum, ACC, dmPFC, SMA, parietal and visual cortex.

Table 1. Whole-brain correlation with adaptive performance for the two choice contrasts

A. Disadvantageous > Advantageous

Cluster Location (BA)	Side	Talairach Coordinates			Probability	Size
		x	y	z		
Medial/superior frontal gyrus (8,6)	R	4	26	42	<0.001	70
Fusiform/middle temporal gyrus (20,21)	R	51	-33	-18	<0.001	14
Anterior cingulate (24)	R	18	11	31	0.001	12
Supramarginal gyrus/precuneus (40,39)	L	-40	-48	26	<0.001	11
Middle frontal gyrus (9)	R	40	33	31	<0.001	11
Middle/medial frontal gyrus (11)	R	25	37	-13	0.004	7

B. Advantageous > Disadvantageous

Cluster Location (BA)	Side	Talairach Coordinates			Probability	Size
		x	y	z		
Superior/inferior frontal gyrus (9,44); anterior cingulate (24); postcentral gyrus (1,2); superior temporal gyrus (22); insula; thalamus	L	-22	44	26	<0.001	710
Medial frontal gyrus (6)	L/R	0	-15	48	<0.001	59
Precuneus (7)	L	-22	-59	48	<0.001	50
Cerebellum, posterior lobe	L	-29	-63	-35	<0.001	27
Postcentral gyrus (3)	R	51	-7	42	<0.001	24
Medial frontal gyrus (10)	L	-4	59	15	<0.001	23
Superior temporal gyrus (42)	R	54	-30	15	<0.001	23
Middle temporal gyrus (21)	R	58	-22	-2	<0.001	22
Postcentral gyrus (43)	R	58	-7	20	<0.001	21
Cerebellum, anterior lobe	L	-22	-41	-18	<0.001	19
Amygdala	L	-29	-4	-13	<0.001	19
Cerebellum, posterior lobe	L	-14	-63	-24	<0.001	15
Middle frontal gyrus (6)	R	36	-7	42	0.001	14
Postcentral gyrus (3)	L	-47	-11	48	<0.001	14
Brainstem, pons	R	7	-22	-29	<0.001	13
Cuneus	L	-18	-78	15	0.001	13
Cerebellum, anterior lobe	R	7	-56	-13	<0.001	12
Middle frontal gyrus (10,46)	L	-29	44	4	<0.001	12
Cerebellum, anterior lobe	R	25	-52	-13	<0.001	11
Midbrain	L	0	-33	-2	0.003	11
Posterior cingulate (30)	L	-7	-56	9	<0.001	11

Whole-brain correlation of activation with net score for the choice phase contrasts: (A) disadvantageous > advantageous choices, (B) advantageous > disadvantageous choices. Unless otherwise stated, only clusters comprising more than 10

voxels are presented. BA: Brodmann's area. Talairach coordinates shown for the peak of each 3D cluster. Probability: cluster-wise correlation probability. Size: number of activated voxels per 3D cluster.

Table 2. Whole-brain correlation with performance for the two outcome contrasts, before and after modulation by expectancy

A. Main Outcome Contrast

Cluster Location (BA)	Side	Talairach Coordinates			Probability	Size
		x	y	z		
Win > Loss						
Superior frontal gyrus (6)	L/R	0	7	48	<0.001	81
Middle frontal gyrus (6)	L/R	-33	7	48	<0.001	57
Thalamus	L/R	0	-7	9	<0.001	55
Postcentral gyrus (2,3)	L	-36	-22	42	<0.001	34
Middle temporal gyrus (39)	R	33	-70	9	<0.001	32
Precuneus (7)	R	4	-70	42	<0.001	27
Supramarginal gyrus (40)	R	47	-48	26	<0.001	24
Caudate body	L	-18	-7	9	<0.001	15
Posterior cingulate (30)	L	0	-44	15	<0.001	14
Caudate body, putamen, thalamus	R	29	-7	-7	<0.001	12
Loss > Win						
Middle frontal gyrus (10)	R	18	52	4	<0.001	43
Posterior cingulate/precuneus (31)	R	18	-41	31	<0.001	31
Middle temporal gyrus (21)	L	-36	-22	-7	<0.001	29
Inferior frontal gyrus (45)	R	36	19	9	<0.001	27
Posterior cingulate (29)	R	22	-37	9	<0.001	14
Insula	R	33	11	9	<0.001	13
Cerebellum, anterior lobe	R	14	-52	-13	<0.001	12
Precentral gyrus (6)	R	29	-7	26	<0.001	12

B. Outcome Contrast Modulated by Positive Expectancy

Cluster Location (BA)	Side	Talairach Coordinates			Probability	Size
		x	y	z		
Win > Loss						
Anterior cingulate (24,32)	L/R	7	-4	37	<0.001	61
Precuneus (7)	R	4	-78	37	<0.001	16
Supramarginal gyrus (40)	R	51	-56	31	<0.001	16
Caudate nucleus	R	11	7	9	<0.001	14
Insula	R	36	-7	-2	<0.001	13
Loss > Win						
Middle frontal gyrus (46)	L	-29	22	20	<0.001	10
Middle frontal gyrus (46)	R	29	33	20	<0.001	7
Cerebellum, posterior lobe	R	29	-52	-35	<0.001	5

C. Outcome Contrast Modulated by Negative Expectancy

Cluster Location (BA)	Side	Talairach Coordinates			Probability	Size
		x	y	z		
Win > Loss						
Middle temporal gyrus (21)	L	-43	-41	-7	0.001	5
Loss > Win						
Precuneus (7)	R	14	-59	26	<0.001	41
Insula; inferior frontal gyrus (45)	R	25	19	-13	<0.001	40
Thalamus	L	-11	-11	-13	<0.001	28
Fusiform gyrus (37)	R	51	-56	-13	<0.001	26
Medial frontal gyrus (6)	R	11	-4	48	<0.001	26
Inferior frontal gyrus (10); anterior cingulate (24,32)	R	25	30	-2	<0.001	23
Middle frontal gyrus (6)	R	36	7	48	<0.001	18
Middle frontal gyrus (6)	R	25	15	53	<0.001	12
Middle/medial frontal gyrus (11)	R	22	41	-13	<0.001	11

Whole-brain correlation of activation with net score for (A) the outcome contrasts (win>loss and loss>win), (B) the outcome contrasts as modulated by positive EV, and (C) the outcome contrasts as modulated by negative EV. Unless otherwise stated, only clusters comprising more than 10 voxels are presented. BA: Brodmann's area. Talairach coordinates shown for the peak of each 3D cluster. Probability: cluster-wise correlation probability. Size: number of activated voxels per 3D cluster.

REFERENCES

Brammer MJ, Bullmore ET, Simmons A, Williams SC, Grasby PM, Howard RJ, Woodruff PW, Rabe-Hesketh S (1997) Generic brain activation mapping in functional magnetic resonance imaging: a nonparametric approach. Magn Reson Imaging 15:763-770.

Bullmore E, Long C, Suckling J, Fadili J, Calvert G, Zelaya F, Carpenter TA, Brammer M (2001) Colored noise and computational inference in neurophysiological (fMRI) time series analysis: resampling methods in time and wavelet domains. Hum Brain Mapp 12:61-78.

Bullmore ET, Suckling J, Overmeyer S, Rabe-Hesketh S, Taylor E, Brammer MJ (1999a) Global, voxel, and cluster tests, by theory and permutation, for a difference between two groups of structural MR images of the brain. IEEE Trans Med Imaging 18:32-42.

Bullmore ET, Brammer MJ, Rabe-Hesketh S, Curtis VA, Morris RG, Williams SC, Sharma T, McGuire PK (1999b) Methods for diagnosis and treatment of stimulus-correlated motion in generic brain activation studies using fMRI. Hum Brain Mapp 7:38-48.

Lawrence NS, Jollant F, O'Daly O, Zelaya F, Phillips ML (2008) Distinct Roles of Prefrontal Cortical Subregions in the Iowa Gambling Task. Cereb Cortex.

Talairach J, Tournoux P (1988) Co-planar stereotaxic atlas of the brain. New York: Thieme.

Zhang H, Nichols TE, Johnson TD (2009) Cluster mass inference via random field theory. Neuroimage 44:51-61.